ELSEVIER

Chemical Geology 203 (2004) 153–168

CHEMICAL GEOLOGY
INCLUDING
ISOTOPE GEOSCIENCE

www.elsevier.com/locate/chemgeo

Carbon–sulfur–iron relationships in sedimentary rocks from southwestern Taiwan: influence of geochemical environment on greigite and pyrrhotite formation

Shuh-Ji Kao[a,*], Chorng-Shern Horng[a], Andrew P. Roberts[b], Kon-Kee Liu[c,d]

[a] *Institute of Earth Sciences, Academia Sinica, Taiwan, ROC*
[b] *School of Ocean and Earth Science, University of Southampton, Southampton Oceanography Centre, Southampton, UK*
[c] *Institute of Hydrological Science, National Central University, Jung-li, Taiwan, ROC*
[d] *National Center for Oceanography Research, National Science Council, Taipei, Taiwan, ROC*

Received 3 February 2003; accepted 30 September 2003

Abstract

The importance of the magnetic iron sulfide minerals, greigite (Fe_3S_4) and pyrrhotite (Fe_7S_8), is often underappreciated in geochemical studies because they are metastable with respect to pyrite (FeS_2). Based on magnetic properties and X-ray diffraction analysis, previous studies have reported widespread occurrences of these magnetic minerals along with magnetite (Fe_3O_4) in two thick Plio-Pleistocene marine sedimentary sequences from southwestern Taiwan. Different stratigraphic zones were classified according to the dominant magnetic mineral assemblages (greigite-, pyrrhotite-, and magnetite-dominated zones). Greigite and pyrrhotite are intimately associated with fine-grained sediments, whereas magnetite is more abundant in coarse-grained sediments. We measured total organic carbon (TOC), total sulfur (TS), total iron (Fe_T), 1N HCl extractable iron (Fe_A), and bulk sediment grain size for different stratigraphic zones in order to understand the factors governing the formation and preservation of the two magnetic iron sulfide minerals. The studied sediments have low TS/Fe_A weight ratios (0.03–0.2), far below that of pyrite (1.15), which indicates that an excess of reactive iron was available for pyritization. Observed low TS (0.05–0.27%) is attributed to the low organic carbon contents (TOC = 0.25–0.55%), which resulted from dilution by rapid terrigenous sedimentation. The fine-grained sediments also have the highest Fe_T and Fe_A values. We suggest that under conditions of low organic carbon provision, the high iron activity in the fine-grained sediments may have removed reduced sulfur so effectively that pyritization was arrested or retarded, which, in turn, favored preservation of the intermediate magnetic iron sulfides. The relative abundances of reactive iron and labile organic carbon appear to have controlled the transformation pathway of amorphous FeS into greigite or into pyrrhotite. Compared to pyrrhotite-dominated sediments, greigite-dominated sediments are finer-grained and have higher Fe_A but lower TS. We suggest that diagenetic environments with higher supply of reactive iron, lower supply of labile organic matter, and, consequently, lower sulfide concentration result in relatively high Eh conditions, which favor formation of greigite relative to pyrrhotite.

Keywords: Greigite; Pyrrhotite; Iron sulfide; Magnetic minerals; Magnetite; Taiwan

* Corresponding author. P.O. Box 1-55, Nankang, Taipei, Taiwan, ROC.
E-mail address: sjkao@earth.sinica.edu.tw (S.-J. Kao).

0009-2541/$ - see front matter © 2003 Elsevier B.V. All rights reserved.
doi:10.1016/j.chemgeo.2003.09.007

1. Introduction

Sedimentary greigite (Fe_3S_4) and pyrrhotite (Fe_7S_8) have received less attention in the literature than pyrite (FeS_2) because they are considered metastable (Sweeney and Kaplan, 1973; Berner, 1984; Wilkin and Barnes, 1997) and are not expected to survive over long periods of geological time. However, these minerals are both strongly magnetic and can be paleomagnetically important. Many rock magnetic studies indicate that greigite and pyrrhotite can be well preserved in sediments with ages ranging from Cretaceous to Holocene (Linssen, 1988; Snowball and Thompson, 1988, 1990; Hilton, 1990; Kalcheva et al., 1990; Krs et al., 1990; Snowball, 1991; Tric et al., 1991; Horng et al., 1992a,b, 1998; Mary et al., 1993; Roberts and Turner, 1993; Hallam and Maher, 1994; Reynolds et al., 1994; Florindo and Sagnotti, 1995; Jelinowska et al., 1995; Roberts et al., 1996; Dinarès-Turell and Dekkers, 1999; Sagnotti and Winkler, 1999; Jiang et al., 2001; Weaver et al., 2002). Despite increasing recognition of their importance, geochemical data based on stratigraphic occurrences of these two iron sulfide minerals are sparse (Reynolds et al., 1994 provide one exception), and the mechanisms responsible for their formation and preservation in natural sedimentary environments are still poorly known (e.g., Morse et al., 1987; Benning et al., 2000).

In southwestern Taiwan, extraordinarily thick (>3000 m) Plio-Pleistocene marine sedimentary sequences, which are composed mainly of massive mudstone and muddy siltstone, are well exposed. In this region, widespread occurrences of authigenic greigite and pyrrhotite, which sometimes coexist with detrital magnetite, have been reported in an area of 600 km^2 (Horng et al., 1992a,b). The existence of greigite and pyrrhotite in these sediments indicates that the pyritization reactions were not completed during early diagenesis. In addition, pyrrhotite and greigite appear in strata with different lithologies. It is likely that different geochemical conditions favor greigite or pyrrhotite formation, respectively (Horng et al., 1992a). In this study, we measured total organic carbon (TOC), total sulfur (TS), total iron (Fe_T), total acid extractable iron (Fe_A), and sediment grain size in bulk samples from two sedimentary sections, where different magnetic mineral assemblages occur (Horng et al., 1992a; Torii et al., 1996). The main goal of this paper is to examine the geochemistry of these magnetic iron sulfide mineral occurrences and to investigate the poorly understood conditions responsible for their formation and preservation.

2. Geological background

The Tsengwen-chi (TW) and Erhjen-chi (EJ) river sections are two representative Plio-Pleistocene marine sequences that crop out in the foothill belt of southwestern Taiwan (Fig. 1a). Horng et al. (1992a) reported three magnetic minerals, greigite, pyrrhotite, and magnetite, which were identified using X-ray diffraction analysis on magnetic extracts from bulk sediments from the two sections. Based on the dominant magnetic mineral occurrences, Horng et al. (1992a) recognized five and three magnetic mineral zones in the TW and EJ sections, respectively. The occurrences of these magnetic minerals are intimately associated with lithological variations (Fig. 1b). Magnetite is dominant in sandstone, greigite is prevalent in mudstone, and pyrrhotite preferentially occurs in muddy siltstone. The presence of detrital magnetite (Horng et al., 1998) suggests that it survived early diagenetic dissolution (Canfield and Berner, 1987), while greigite and pyrrhotite are authigenic minerals that formed after sediment deposition. In the case of greigite, an authigenic origin is well supported by the studies of Horng et al. (1998) and Jiang et al. (2001). Studies of the pyrrhotite in these sediments

Fig. 1. (a) Generalized geological map of Taiwan. The dashed line indicates the boundary between the Philippine Sea Plate and the Eurasian Plate. The Tsengwen-chi (TW) and Erhjen-chi (EJ) sections of the western foothill belt are located about 30 km to the northeast and southeast of Tainan City, respectively. (b) Detailed map of the TW and EJ sections, showing lithological formations, nannofossil biochronology, magnetic mineral zones (P: pyrrhotite, G: greigite, and M: magnetite) (see Horng et al., 1992a,b), and sampling sites used for geochemical analyses in this study (black dots). Five and three magnetic mineral zones are recognized in the TW and EJ sections, respectively (see text).

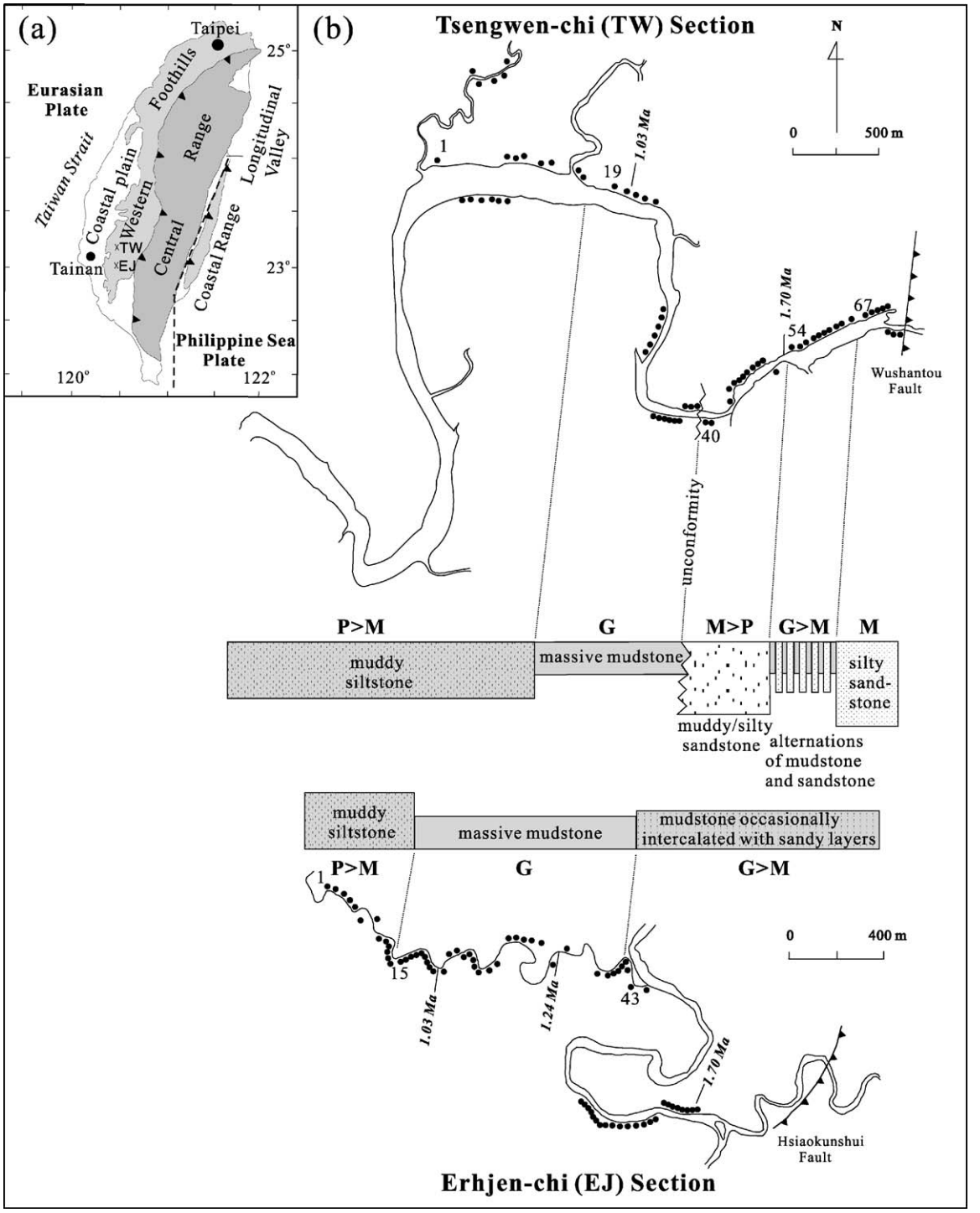
(a)
Taipei
25°
Eurasian Plate
Foothills
Longitudinal Valley
Taiwan Strait
Coastal plain
Western
Range
Central
Coastal Range
TW
EJ
Tainan
23°
Philippine Sea Plate
120°
122°
(b)
Tsengwen-chi (TW) Section
N
0
500 m
1
19
1.03 Ma
1.70 Ma
54
67
Wushantou Fault
40
unconformity
P>M
G
M>P
G>M
M
muddy siltstone
massive mudstone
silty sand-stone
muddy/silty sandstone
alternations of mudstone and sandstone
muddy siltstone
massive mudstone
mudstone occasionally intercalated with sandy layers
P>M
G
G>M
1
0
400 m
15
1.03 Ma
1.24 Ma
43
1.70 Ma
Hsiaokunshui Fault
Erhjen-chi (EJ) Section

are ongoing; however, preliminary petrographic studies indicate the presence of pyrrhotite nodules and individual grains with textures that are consistent with in situ authigenic growth. For example, Horng et al. (1998) reported the presence of euhedral pyrrhotite grains that were unlikely to have retained their sharp crystal habit during sediment transportation. We therefore assume that the pyrrhotite in the studied sediments has an authigenic origin. The data presented here provide the first detailed geochemical analysis of stratigraphic sequences containing greigite and pyrrhotite.

On the basis of nannofossil biochronology (Torii et al., 1996; Horng et al., 1998), the sedimentation rates ranged from 280 to 380 cm ky^{-1} for the TW section and from 150 to 200 cm ky^{-1} for the EJ section. The high sedimentation rates are due to the tremendous southward dumping of sediment from the Central Range into an ancient foreland basin. The Central Range rapidly uplifted as a result of collision between the Philippine Sea Plate and the Eurasian Continental Plate during the Plio-Pleistocene (Fig. 1a). The sediments were mainly sourced from the northern region. The TW section therefore has more coarse-grained sandstones and a higher concentration of magnetite than the EJ section. From Fig. 1b, it should be noted that the upper two magnetic mineral zones for the two sections are coeval and can be correlated on the basis of lithology.

3. Materials and methods

A total of 73 and 71 samples covering different magnetic mineral zones were collected from the TW and EJ sections, respectively. Details about the magnetic properties of these sediments have been reported by Horng et al. (1992b) and Torii et al. (1996). The sampling locations are shown in Fig. 1b. Note that TOC and total sulfur (TS) were measured for all samples, but only selected samples were measured for iron contents (Table 1 and Appendix A and B).

Samples were dried and thoroughly crushed into powders for geochemical analysis. About 0.1 g of sediment was fumed with HCl to remove inorganic carbon for TOC analysis. The decarbonated samples were analyzed for carbon content with a LECO WR112 carbon analyzer. The relative precision for TOC analysis is better than 5%. TS was determined with a HORIBA EMIA model CS500 analyzer with a resistance furnace and a ND-IR detector. About 0.2 g of sample, mixed with 1 g of granular tin, was combusted in the analyzer to produce SO_2 at 1350 °C. At this temperature, all sulfide minerals including pyrite are oxidized to form SO_2. The relative precision for TS analysis is better than 1%.

Cold acid extractable iron (Fe_A) was extracted by adding 15 ml of 1N HCl to 50 mg of sample which was reacted for 16 h with continuous stirring (Lin and Morse, 1991). This operationally defined fraction represents the maximum value of reactive iron in the sediments (Raiswell et al., 1994). For the determination of total iron concentration (Fe_T), samples were digested with a 2:5 mixture of concentrated HF and HNO_3 (Kokot et al., 1992). The solutions from extraction or digestion were analyzed for Fe_A and Fe_T with a Hitachi-Z8100 flame atomic absorption spectrometer. Standards

Table 1
Summary of mean weight percent ± standard deviation for the measured geochemical properties from the TW and EJ sections

Section	Mag. min. zone	TOC (%)	Fe_T (%)	Fe_A (%)	TS (%)
TW	P>M	0.37 ± 0.05(18)	3.39 ± 0.26(6)	1.80 ± 0.19(6)	0.16 ± 0.05(18)
	G	0.46 ± 0.04(21)	4.06 ± 0.15(6)	2.15 ± 0.18(6)	0.13 ± 0.03(21)
	M>P	0.29 ± 0.06(14)	3.26 ± 0.39(6)	1.68 ± 0.14(6)	0.14 ± 0.04(14)
	G>M	0.36 ± 0.05(12)	3.81 ± 0.30(5)	2.15 ± 0.34(5)	0.09 ± 0.01(12)
	M	0.32 ± 0.03(8)	3.26 ± 0.24(4)	1.82 ± 0.09(4)	0.07 ± 0.01(8)
EJ	P>M	0.33 ± 0.07(14)	3.44 ± 0.50(8)	1.87 ± 0.24(8)	0.13 ± 0.06(14)
	G	0.47 ± 0.06(28)	4.55 ± 0.35(15)	2.32 ± 0.19(15)	0.11 ± 0.03(28)
	G>M	0.46 ± 0.05(29)	4.31 ± 0.59(7)	2.12 ± 0.41(7)	0.10 ± 0.03(29)

Numbers in parentheses indicate the number of samples that were analyzed from individual magnetic mineral zones.

used for calibration were prepared with the same matrix. Accuracy and precision were checked by replicate analysis of total metal concentrations in standard reference material BCSS-1 (National Research Council, Canada), following total digestion. The certified value and our measurement of iron content are $3.287 \pm 0.098\%$ and $3.266 \pm 0.056\%$ ($n = 5$), respectively (data published in Hsu et al., in press). The accuracy for iron analysis was better than 1%. The relative standard deviation for field samples (iron concentrations ranged from ~2% to 5%) in this study was better than 5%.

Grain size analysis for different magnetic mineral zones was performed using large (>100 g) bulk sediment samples that were mechanically sieved into three size fractions: >63 μm (sand), 45–63 μm (coarse silt), and <45 μm (medium silt to clay). Each fraction was weighed. The finest fraction was further analyzed with a Galai CIS-1 laser beam particle sizer and was subdivided into three particle grades: 20–45 μm (medium silt), 5–20 μm (fine silt), and <4 μm (clay). Details of the procedures are given by Tsai and Rau (1992). The volume-based size distribution data were transformed to dry weight percentages based on the average density of the samples.

4. Results

Stratigraphic variations of TOC, Fe_A, Fe_T, and TS for the TW and EJ sections are shown in Figs. 2 and 3, respectively. The full data sets for the two sections are listed in Appendix A. The mean values and the

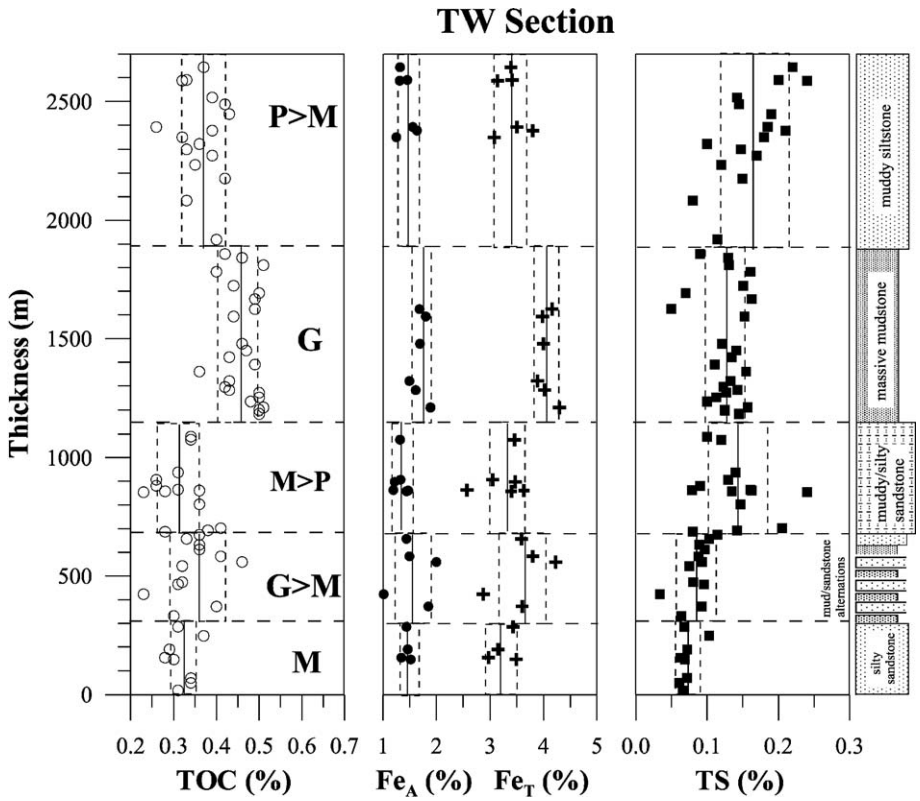

Fig. 2. Concentrations of TOC (○), Fe_A(●), Fe_T (+), and TS (■) for samples from the five magnetic mineral zones of the TW section. The mean values ± 1 standard deviation are shown for each magnetic mineral zone by the solid and dashed lines, respectively. A lithological column is shown on the right-hand side.

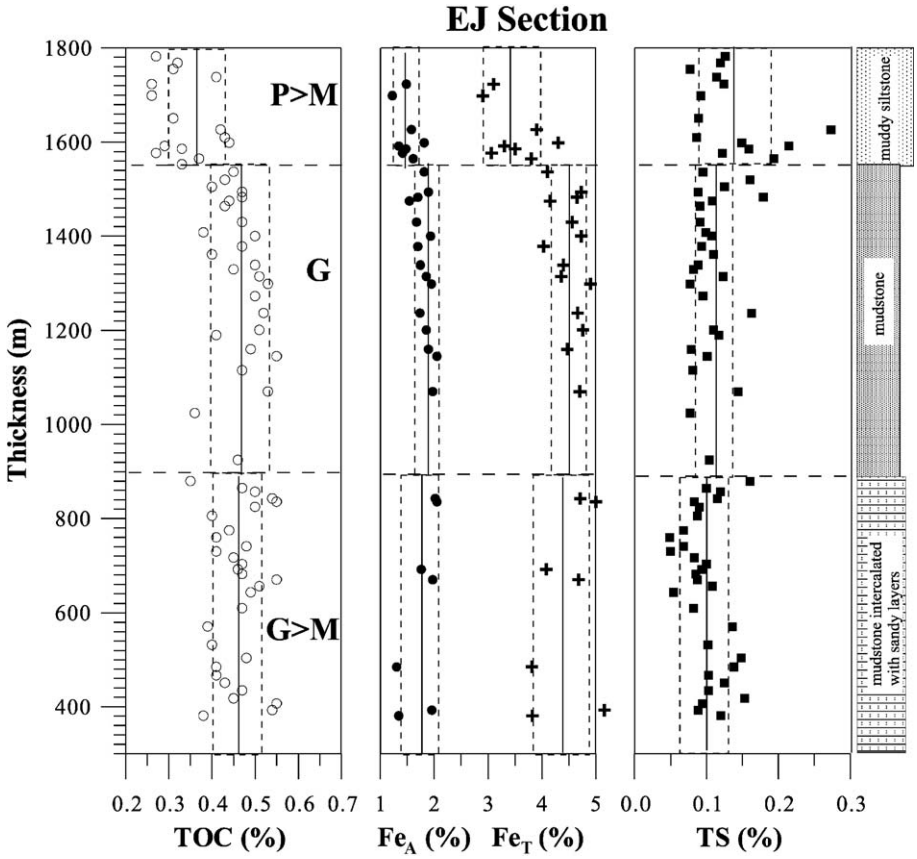

Fig. 3. Stratigraphic variations of C–Fe–S for the EJ section. Symbols are the same as in Fig. 2.

standard deviations of these parameters are summarized in Table 1.

TOC values for the two sections range from 0.17% to 0.55% (Figs. 2 and 3). Most greigite-dominated zones, i.e., the zone marked with G in the TW section (Fig. 2) and zones marked with G or G>M in the EJ section (Fig. 3), have higher mean TOC values (0.46–0.47%) than other zones (0.29–0.37%). An exception is the zone marked G>M in the TW section, where the mean TOC value is only $0.36 \pm 0.05\%$ (Table 1). This exception is caused by the intercalation of mudstones and sandstones; we attribute the low TOC value to the sandstones, whereas greigite mainly occurs in the mudstones.

The TS contents for the two sections range from 0.05% to 0.27% (Figs. 2 and 3). It is the pyrrhotite-dominated zones, rather than the greigite-dominated zones, that have higher mean TS values (see also Fig. 5b). The magnetite-dominated zones have the lowest concentrations of both TOC and TS (see also Fig. 5b), but the TS contents become higher in samples with occurrences of pyrrhotite as a minor magnetic mineral (M>P zone in the TW section; Table 1).

The Fe_T concentrations from the two sections fall within the range from 2.5% to 5.2% (Figs. 2 and 3). These values fall in the reported range (0.8–7.6%) of total iron expected in shales (Davis et al., 1988) and are similar to those reported for continental margins in the compilation by Raiswell and Canfield (1998). Fe_T concentrations vary in phase with TOC variations (Figs. 2 and 3), and there is a tight linear correlation between these two parameters

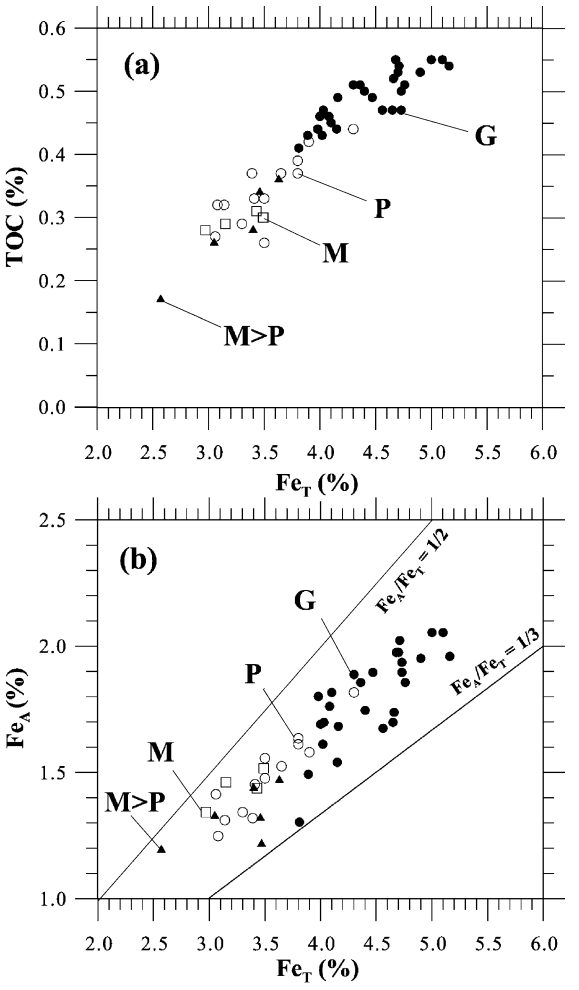

Fig. 4. Plots of (a) TOC versus Fe_T and (b) Fe_A versus Fe_T for greigite- (●), pyrrhotite- (○), and magnetite- (□) dominated zones from the TW and EJ sections, which are clearly linearly related. Samples in the M>P zone (▲) are also shown (see text). The Fe_A/Fe_T ratios of 1/2 and 1/3 are shown as lines.

(Fig. 4a). Fe_A values also correlate well with Fe_T values (Fig. 4b). About 40% of the Fe_T can be extracted as Fe_A. Contrary to these correlations, neither Fe_T, Fe_A, nor TOC values are positively correlated with TS values (Fig. 5). All observed TS/Fe_A ratios (0.03–0.2; Fig. 5a) are far below that of saturated pyrite (TS/Fe = 1.15). This reflects a low degree of pyritization with limited sulfur-bound iron in all samples. Pyrrhotite-dominated samples have relatively high TS/Fe_A ratios (Fig. 5a), but these ratios are still considerably lower than the stoichiometric ratio of any iron sulfide mineral. Moreover, greigite-dominated samples have TS/Fe_A ratios that are mostly lower than 0.1 (Fig. 5a), which indicates that much more excess reactive iron was available than in pyrrhotite-dominated environments. Magne-

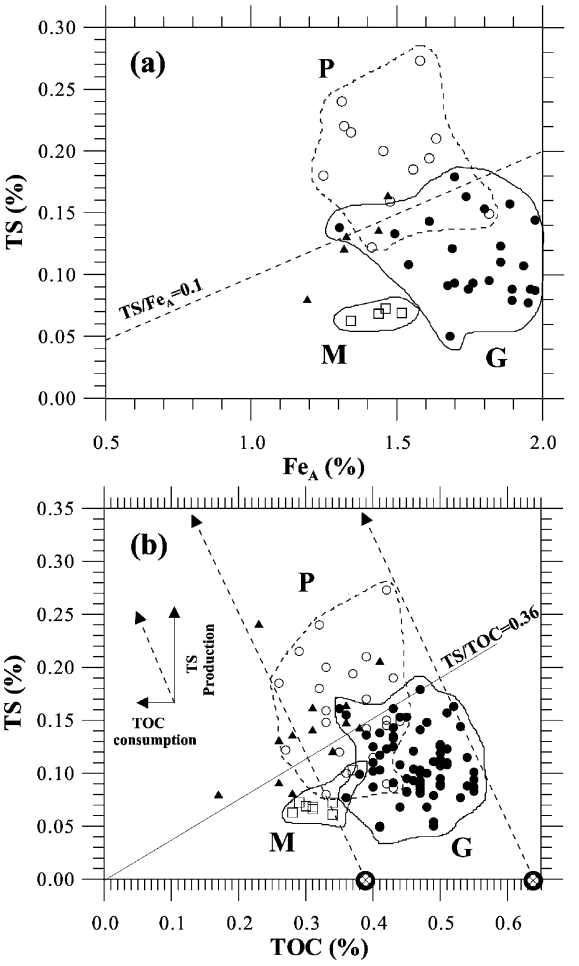

Fig. 5. Plots of (a) TS versus Fe_A and (b) TS versus TOC for different magnetic mineral zones from the TW and EJ sections. Symbols are the same as in Fig. 4. The line for a TS/Fe_A ratio of 0.1 is shown in (a). Two dashed lines in (b) represent the evolving loci of TS production as TOC is decomposed via sulfate reduction (see text). A TS/TOC ratio of 0.36, which is the global average in normal marine sediments (Berner and Raiswell, 1983; Raiswell and Berner, 1986), is shown. Filled circles on the *x*-axis mark two hypothetical TOC_I values that span the range of values for the data from the TW and EJ sections.

tite-dominated zones have the lowest TS/Fe_A ratios (Fig. 5a).

The lack of correlation between TS and TOC values in our samples (Fig. 5b) is in contrast to the normally expected positive relationship (Berner and Raiswell, 1983; Raiswell and Berner, 1986). In Fig. 5b, the data points from pyrrhotite-dominated zones are mostly higher than the global average TS/TOC ratio of 0.36 in normal (oxic and normal seawater salinity) marine sediments, whereas those from greigite-dominated zones are almost all below the global average. Those from magnetite-dominated zones are clustered at the lowest TOC and TS concentrations.

The average grain size distributions of the greigite-, pyrrhotite-, and magnetite-dominated zones in the two studied sedimentary sections are presented in Table 2. In Fig. 6, the mean weight percentage for each of the five size fractions is plotted for the three types of magnetic mineral zones, which enables a comparison of the relative importance of each size fraction in the three types of sediments. The two finest size fractions (clay and fine silt) are most abundant in the greigite-dominated sediments and are least abundant in the magnetite-dominated sediments. For the two coarsest size fractions (coarse silt and sand), the trend is reversed. For the intermediate size fraction (medium silt), the abundances are similar among the three types of sediments.

Table 2.
Grain size data for bulk sediments from greigite-, pyrrhotite-, and magnetite-dominated zones of the TW and EJ sections

Site	<4 μm clay	5–20 μm fine silt	20–45 μm medium silt	45–63 μm coarse silt	>63 sand
Greigite-dominated zones					
TW19	30	54	12	2	2
TW23	13	49	24	7	7
TW26	17	65	13	3	2
TW30	18	41	32	6	3
TW35	12	53	31	2	2
EJ18	20	57	19	2	2
EJ31	22	60	13	2	3
EJ36	14	42	43	1	1
EJ39	18	64	12	3	3
Average	18 ± 5	54 ± 9	22 ± 11	3 ± 2	3 ± 2
Pyrrhotite-dominated zones					
TW01	7	30	30	15	18
TW04	10	46	21	11	11
EJ02	12	38	39	3	9
EJ04	12	41	33	3	10
EJ08	12	42	19	8	19
EJ12	10	43	38	1	9
Average	11 ± 2	40 ± 6	30 ± 8	7 ± 5	13 ± 5
Magnetite-dominated zones					
TW62	4	28	18	11	40
TW64	1	20	40	16	23
TW66	3	24	22	19	32
TW67	2	14	16	8	60
Average	3 ± 1	22 ± 6	24 ± 11	14 ± 5	39 ± 16

The values are mean weight percentages for each size fraction.

The greigite-dominated sediments contain about 50% fine silt, which is by far the most abundant fraction. It is also the most abundant fraction in pyrrhotite-dominated sediments, but it is not as dominant as in greigite-dominated sediments. The magnetite-dominated sediments contain about 30% sand and little clay. It is clear that greigite occurrences are associated with fine-grained sediments, magnetite with coarse-grained sediments, and pyrrhotite with medium-grained sediments. This trend is consistent with the qualitative relationship between lithology and magnetic mineral assemblage described by Horng et al. (1992a). This trend also confirms the suggestion by Horng et al. (1992a) that magnetite has undergone dissolution in the fine-grained sediments (Canfield and Berner, 1987; Canfield et al., 1992).

5. Discussion

In light of our geochemical data, we discuss the conditions required for the preservation of these metastable iron sulfide assemblages and factors that might control the transformation of iron sulfide precipitates into greigite or pyrrhotite.

5.1. Rapid sedimentation and arrest of pyritization

In the marine environment, the relative rates of supply of organic matter, sulfate, and reactive iron, which are all related to the sedimentation rate, ultimately control pyrite formation or the lack of it, which is known as the arrest of pyritization (Goldhaber and Kaplan, 1974; Morse et al., 1987;

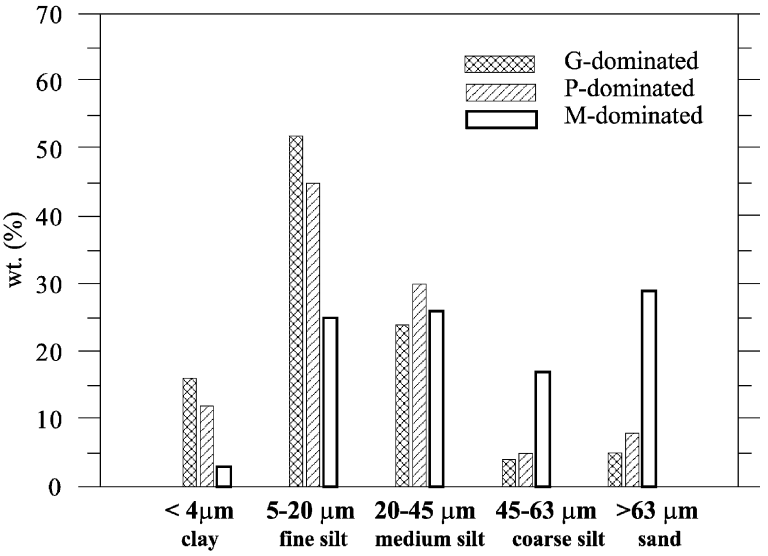

Fig. 6. Mean grain size distributions of sediments from the greigite-, pyrrhotite-, and magnetite-dominated zones of the TW and EJ sections. Data are from the averages listed in Table 2.

Wilkin and Barnes, 1997). During diagenesis, greigite and pyrrhotite are metastable in the presence of excess H_2S and are expected to eventually transform into pyrite (Berner, 1967). However, these intermediate phases may be preserved if the pyritization process is arrested due to insufficient supply of H_2S (Berner et al., 1979). Though the dominant reaction pathways of pyrite formation remain controversial, most studies have indicated that pyritization requires addition of elemental sulfur to the metastable iron sulfides (e.g., Sweeney and Kaplan, 1973; Benning et al., 2000 and references therein). The production of elemental sulfur via oxidation of sulfide ions is a slow process compared to precipitation of iron sulfide, which does not involve electron transfer. Therefore, the presence of elemental sulfur, which appears to be the key factor in controlling pyrite formation, requires accumulation of hydrogen sulfide. If the rate of H_2S supply is slow, then all reduced sulfur can be fixed as iron sulfide as soon as it is produced, and there is little chance for it to be converted to elemental sulfur. Laboratory experiments have confirmed this view (Schoonen and Barnes, 1991a,b).

In the case of the sediments studied here, the cause of the insufficient supply of H_2S, which resulted in the widespread preservation of metastable iron sulfides, appears to be associated with low TOC contents coupled with a high percentage of reactive iron (Fe_A) in the rapidly deposited sediments. These features are a natural consequence of erosion and sedimentation in an active orogenic margin. Denudation of the rapidly uplifted Central Range and bulging of the foreland favors rapid erosion, which has generated a high flux of lithogenic materials, and thus high sedimentation rates, in the surrounding depositional environments. Similar processes are still active and sedimentation rates reported for modern sediments around southwestern Taiwan range from 50 to 750 cm ky^{-1} at water depths of 100–2700 m (Chen and Leu, 1984; Tsai and Chung, 1989; Lee et al., 1993).

Sedimentation rate can have both positive (preservational) and negative (diluent) effects on sedimentary TOC contents. Based on modeling results, Tyson (2001) suggested that sedimentation rate could enhance TOC content only at rates <5 cm ky^{-1} in oxic environments. Dilution dominates at higher rates. The materials contributing to TOC dilution in our case are mainly terrigenous minerals rather than carbonate, as indicated by $CaCO_3$ contents of $<8\%$ ($n=285$, unpublished data) for the

two studied sections. The rather low TOC values (0.17–0.55%) relative to the expected range of TOC values in normal mud rocks (0.7–1.2%; Blatt et al., 1984) can therefore be attributed to mineral dilution. Such low TOC contents will result in relatively low rates of H_2S production, which explains the low TS contents observed throughout the studied sections.

The balance between supply of available iron and labile organic matter can regulate the H_2S concentration in porewater. A rich supply of reactive iron effectively removes H_2S and keeps the H_2S supply low, which will arrest pyritization. We have demonstrated that Fe_A is in great excess with respect to the amount needed for the formation of pyrite in our samples. However, different iron-bearing minerals have different reactivities toward sulfide (Canfield, 1989; Canfield et al., 1992; Raiswell and Canfield, 1996). The cold HCl technique used in this study has limitations because it may not dissolve some iron oxide minerals and can extract small amounts of additional iron from silicate minerals (Raiswell et al., 1994). Tseng (1991) showed that there is a good correlation among easily reducible iron, total iron, and the fine fraction in modern surface marine sediments around Taiwan. Within his samples, about 40% of Fe_T was easily to moderately reducible, as represented by the first four stages in the six-stage sequential extraction procedure defined by Chester et al. (1988). This result agrees with our observations of the fraction of Fe_A in Fe_T in the studied Plio-Pleistocene sediments. In addition, Huang and Lin (1995) studied marine sediments north of Taiwan and showed that they contain abundant oxalate extractable iron (mainly ferrihydrite and lepidocrocite; Canfield et al., 1992), which is highly reactive toward sulfide (half-life of hours to days) and which results in undetectable porewater H_2S in sediments undergoing active sulfate reduction. It is therefore reasonable to assume that even though the cold HCl technique used in this study has limitations, it still provides evidence that reactive iron was in excess during early diagenesis in sediments throughout the studied sections. The abundant reactive iron coupled with diluted organic matter disables the completion of pyritization and thus benefits the preservation of metastable iron sulfides.

The starvation of sulfate provision due to insufficient sulfate in bottom waters or to diminished sulfate diffusion below the sediment–water interface may also cause incomplete pyritization in sediments. The two studied marine sequences are unlikely to have been limited by sulfate supply in view of the abundant sulfate in seawater. However, high sedimentation rates might lengthen the sulfate diffusion pathway and lead to sulfate starvation. According to Goldhaber and Kaplan (1974), the sedimentation rate must be as high as 30 cm $year^{-1}$ to totally block sulfate diffusion, whereas the rates in the studied sediments were no more than about 0.4 cm $year^{-1}$ (Torii et al., 1996; Horng et al., 1998). Therefore, sulfate limitation is unlikely to have been responsible for arrested pyritization in the two studied sequences.

5.2. Conditions controlling the formation of greigite or pyrrhotite

The distinctive lithological and geochemical characteristics of greigite- and pyrrhotite-dominated zones in the studied sediments indicate that different biogeochemical conditions are required for greigite and pyrrhotite formation. We now discuss potential controls on the preferential transformation from iron sulfide precipitates to greigite or to pyrrhotite. Precipitation of iron sulfides is directly affected by H_2S production and the reactivity of iron toward sulfide. We have suggested above that the availability of organic matter and of ferric iron (as one of the oxidants) are the two most important factors governing the preferential occurrence of one magnetic iron sulfide mineral with respect to the other in our study area.

5.2.1. Supply of organic matter

During sulfate reduction, two molecules of organic C are consumed to produce one molecule of sulfide-S. The weight ratio of S formed to C consumed is 4:3 (1:2 as a molecular ratio). The stoichiometry allows us to back-calculate the demand of TOC (TOC_D) required to produce the measured TS content:

$$TOC_D = TS*3/4. \quad (1)$$

By adding the demand (TOC_D) to the measured value (TOC_M), which is the residual remaining after diage-

netic degradation of organic carbon, we can estimate the initial quantity, TOC_I, as follows:

$$TOC_I = TOC_M + TOC_D. \quad (2)$$

The evolving loci of TOC-TS as a result of diagenetic organic carbon consumption and sulfur production for the range of values bracketing those observed in the studied sediments are shown in Fig. 5b. TOC_I values marked on the *x*-axis may therefore be considered the TOC contents in the sediments at the beginning of sulfate reduction during early diagenesis. The back-calculation reveals that the pyrrhotite-dominated sediments have similar TOC_I values as the greigite-dominated sediments. The higher TS values observed for pyrrhotite-dominated sediments implies higher TOC_D values, which represents a higher labile fraction relative to the greigite-dominated sediments. The higher TOC_M values in greigite-dominated sediments indicate higher contents of refractory organic matter.

The differences in grain size distribution between the greigite- and pyrrhotite-dominated zones suggest that these two authigenic minerals were formed at different water depths. This is supported by recent findings in modern marine sediments offshore of southwestern Taiwan (Horng, unpublished data), where greigite was found in sediments from deeper water depths (500–1500 m) and pyrrhotite was mostly found in sediments from shallower water depths (30–750 m). A difference in water depth is consistent with our inferences concerning the fraction of labile organic matter, which should be greater at shallower depths.

5.2.2. Eh–log [$S^{=}$] diagram

In order to explore the conditions that favor the preferential formation of different magnetic iron sulfide minerals, we use an Eh – log [$S^{=}$] diagram to represent a range of appropriate redox and geochemical conditions (Fig. 7). By assuming a constant pH, we calculated the stability fields of the concerned minerals using thermodynamic properties (Garrels and Christ, 1965; Berner, 1967). The most sulfur-deficient compound, mackinawite ($FeS_{0.9}$), is the first precursor in the iron sulfide formation series

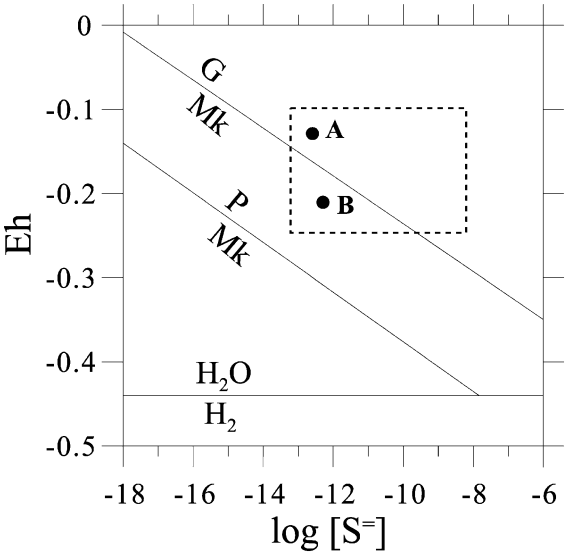

Fig. 7. Eh – log [$S^{=}$] phase diagram for metastable iron sulfides (Berner, 1967) at a constant pH of 7.5. The transformation boundaries from mackinawite (Mk) into greigite (G) or pyrrhotite (P) are shown. The dashed rectangle represents the range of Eh and log [$S^{=}$] values encountered in natural environments from Berner (1964). Points A and B represent two conditions that favor transformation into greigite and pyrrhotite, respectively.

(Sweeney and Kaplan, 1973; Berner, 1984; Morse et al., 1987; Wilkin and Barnes, 1997). The transformation boundary of mackinawite–greigite is toward higher [$S^{=}$] and higher Eh relative to the mackinawite–pyrrhotite transformation boundary. At a given Eh, the transformation into greigite, as compared to that into pyrrhotite, must take place at higher [$S^{=}$], which is opposite to our observation of lower TS in greigite-dominated samples. This implies that the Eh conditions of the diagenetic environments must be quite different for the transformation into greigite or pyrrhotite. In other words, Eh must have been the critical factor that controls the transformation. Higher Eh would favor the transformation into greigite as represented by point A in Fig. 7 (see elaboration below).

For illustration, we plot in Fig. 7 the domain of observed natural Eh – log [$S^{=}$] conditions reported by Berner (1964). This domain covers the stability fields of both pyrrhotite and greigite with respect to mackinawite. In other words, mackinawite is unstable under natural conditions and therefore must

transform into other forms. The differences in natural redox and geochemical conditions of diagenetic environments may result in different stable forms of the two magnetic iron sulfide minerals during the transformation of mackinawite. Under TOC-poor and iron-rich conditions, it is likely that [$S^{=}$] had been maintained at a relatively low value probably within a narrow range. Thus, for transformation into greigite, the environment needs to maintain Eh at a higher level, such as at point A in Fig. 7, whereas the transformation into pyrrhotite requires a condition represented by point B. This agrees with our suggestion of lower fractions of labile organics in greigite-bearing sediments, where ferric iron may have been in excess and maintained a higher Eh. In contrast, the higher fraction of labile organics in the pyrrhotite forming sediments, may have kept Eh at lower level due to the depletion of ferric iron by reacting with the labile organics.

It is inferred from our observations that under TOC-poor conditions, abundant reactive iron not only prevents accumulation of porewater H_2S, but the ferric form of it may also play a role in controlling Eh, and therefore may determine the iron sulfide transformation pathway. Although the standard Gibbs free energy of iron monosulfides has been questioned based on porewater chemistry from field observations (Wilkin and Barnes, 1997), the phase diagram derived from these thermodynamic data does not necessarily contradict our observations. In other words, it is plausible that the redox conditions required by the stability fields of greigite and pyrrhotite could have existed in the sediments with the respective geochemical and lithological characteristics. Future laboratory studies are required to determine robust thermodynamic parameters for these iron sulfide phases to test our hypotheses, and more geochemical data from other locations are needed to better understand the occurrences of greigite and pyrrhotite in sedimentary environments.

6. Conclusions

C–S–Fe relationships in Plio-Pleistocene sediments from southwestern Taiwan indicate that greigite and pyrrhotite are preserved in environments that are poor in TOC and rich in reactive Fe. The limited supply of organic matter and the abundant reactive iron in the rapidly deposited sediments appear to be responsible for effective removal of reduced sulfur by precipitation of intermediate iron sulfides. This has prevented pyritization and, consequently, has resulted in the widespread occurrence of metastable iron sulfide minerals, which are the dominant magnetic minerals in the studied mudstones and siltstones. Remnants of detrital magnetite mainly occur in sandstones, which suggests that magnetite has undergone almost complete dissolution in finer-grained sediments.

Compared to pyrrhotite-dominated sediments, greigite-dominated sediments have more clay, higher concentrations of cold acid extractable iron (Fe_A), higher TOC, and lower TS. Back-calculation suggests that the pyrrhotite-dominated sediments contained similar contents of initial TOC, but a higher labile fraction compared to greigite-dominated sediments. Apparently, variations in sediment grain size, labile organic carbon contents, and reactive iron have controlled which of the two magnetic iron sulfide minerals formed during diagenesis. Combining thermodynamic considerations and evidence from geochemical observations, we conclude that diagenetic conditions with higher Eh must have favored formation of greigite compared to the conditions that gave rise to formation of pyrrhotite. This is consistent with the lower labile organic matter content in greigite-bearing sediments, which has resulted in lower TS contents, and is also consistent with the higher reactive iron contents, of which the ferric fraction probably contributed to maintaining a higher Eh. The finer grain sizes suggest that such diagenetic conditions prevail at greater water depths relative to sediments in which pyrrhotite formed, which is consistent with recent observations of greigite occurrences in modern sediments from offshore of southwestern Taiwan.

Acknowledgements

We thank Hsu, S.-C. (IES, AS, Taiwan), Tsai, C.-H. (NTOU), and Lee, T.-H. (NTU) for assistance

with sampling and chemical analyses. We also thank Dr. L. Sagnotti, Dr. C. J. Allègre, Dr. W.-L. Jeng (NTU), and an anonymous reviewer for constructive comments on an earlier version of this paper. This study was supported by the National Science Council of the Republic of China under grants NSC 89-2611-M-002-041-OP3 to S.J.K. and NSC 90-2911-I-001-010 to C.S.H. and by a grant from the Royal Society of London to A.P.R. This is IESAS contribution number IESAS911 and NCOR contribution number 79. [**CA**]

Appendix A. Geochemical parameters for five subdivisions in the TW section

Thickness (m)	TOC (%)	Fe_T (%)	Fe_A (%)	TS (%)
P>M				
2645	0.37	3.39	1.32	0.22
2591	0.33	3.41	1.45	0.20
2588	0.32	3.14	1.31	0.24
2517	0.39			0.14
2488	0.42			0.15
2447	0.43			0.19
2392	0.26	3.50	1.56	0.19
2377	0.39	3.80	1.64	0.21
2349	0.32	3.08	1.25	0.18
2321	0.36			0.10
2299	0.33			0.15
2273	0.39			0.17
2234	0.35			0.12
2176	0.42			0.15
2083	0.33			0.08
1918	0.40			0.12
1857	0.42			0.09
1841	0.46			0.13
G				
1810	0.51			0.13
1782	0.40			0.16
1723	0.44			0.15
1692	0.50			0.07
1667	0.49			0.16
1624	0.49	4.16	1.68	0.05
1593	0.44	3.98	1.80	0.15
1478	0.46	4.00	1.69	0.12
1449	0.47			0.14
1421	0.43			0.14
G				
1390	0.49			0.11
1360	0.36			0.16
1320	0.43	3.89	1.49	0.13
1295	0.42			0.12
1282	0.43	4.02	1.61	0.14
1271	0.50			0.13
1251	0.50			0.11
1234	0.48			0.10
1209	0.51	4.30	1.89	0.16
1199	0.50			0.13
1184	0.50			0.15
M>P				
1089	0.34			0.10
1076	0.34	3.46	1.32	0.12
938	0.31			0.14
907	0.26	3.05	1.33	0.13
881	0.26			0.09
865	0.31			0.16
861	0.36	3.63	1.47	0.16
858	0.28	3.40	1.44	0.14
854	0.23			0.24
803	0.36			0.15
702	0.41			0.21
693	0.38			0.14
687	0.28			0.08
G>M				
674	0.36			0.12
657	0.33	3.59	1.44	0.10
632	0.36			0.09
612	0.36			0.10
583	0.41	3.80	1.49	0.09
559	0.46	4.23	2.00	0.09
542	0.32			0.08
474	0.32			0.08
465	0.31			0.10
423	0.23	2.87	1.01	0.03
371	0.40	3.60	1.85	0.09
331	0.30			0.06
M				
285	0.31	3.43	1.44	0.07
247	0.37			0.10
190	0.29	3.15	1.46	0.07
155	0.28	2.97	1.34	0.06
147	0.30	3.49	1.52	0.07
70	0.34			0.07
50	0.34			0.06
18	0.31			0.07

Appendix A (*continued*)

Appendix B. Geochemical parameters for three subdivisions in the EJ section

Thickness (m)	TOC (%)	Fe_T (%)	Fe_A (%)	TS (%)
P>M				
1782	0.27			0.13
1768	0.32			0.12
1755	0.31			0.08
1738	0.41			0.11
1723	0.26	3.10	1.49	0.12
1699	0.26	2.90	1.22	0.09
1651	0.31			0.09
1627	0.42	3.90	1.58	0.27
1610	0.43			0.09
1599	0.44	4.30	1.82	0.15
1592	0.29	3.30	1.34	0.22
1586	0.33	3.50	1.48	0.16
1577	0.27	3.06	1.41	0.12
1565	0.37	3.80	1.61	0.19
G				
1553	0.33			0.11
1537	0.45	4.10	1.82	0.10
1520	0.43			0.16
1505	0.40			0.13
1494	0.47	4.73	1.90	0.09
1483	0.47	4.65	1.70	0.18
1475	0.44	4.15	1.54	0.11
1464	0.43			0.09
1430	0.47	4.56	1.67	0.09
1408	0.38			0.10
1400	0.50	4.73	1.94	0.11
1378	0.47	4.03	1.70	0.09
1361	0.40			0.11
1339	0.50	4.40	1.75	0.09
1330	0.45			0.08
1315	0.51	4.36	1.86	0.12
1299	0.53	4.90	1.95	0.08
1273	0.50			0.10
1237	0.52	4.66	1.74	0.16
1201	0.51	4.76	1.86	0.11
1190	0.41			0.12
1160	0.49	4.47	1.90	0.08
1145	0.55	5.10	2.05	0.10
1115	0.47			0.08
1070	0.53	4.70	1.98	0.14
1024	0.36			0.08
925	0.46			0.10
880	0.35			0.16
G>M				
865	0.47			0.10
857	0.50			0.12
843	0.54	4.71	2.02	0.12
836	0.55	5.00	2.05	0.08
825	0.50			0.09
806	0.40			0.09
775	0.44			0.07
760	0.41			0.05
741	0.48			0.07
730	0.41			0.05
717	0.45			0.08
703	0.47			0.10
692	0.46	4.08	1.76	0.09
682	0.47			0.09
670	0.55	4.68	1.98	0.09
656	0.51			0.11
643	0.49			0.05
610	0.47			0.08
571	0.39			0.14
532	0.40			0.10
504	0.48			0.15
485	0.41	3.81	1.30	0.14
467	0.41			0.10
451	0.43			0.13
435	0.47			0.10
418	0.45			0.15
407	0.55			0.09
393	0.54	5.16	1.96	0.09
381	0.38	3.82	1.34	0.12

References

Benning, L.G., Wilkin, R.T., Barnes, H.L., 2000. Reaction pathways in the Fe–S system below 100°C. Chem. Geol. 167, 25–51.

Berner, R.A., 1964. Stability fields of iron minerals in anaerobic marine sediments. J. Geol. 72, 293–306.

Berner, R.A., 1967. Thermodynamic stability of sedimentary iron sulfide. Am. J. Sci. 265, 773–785.

Berner, R.A., 1984. Sedimentary pyrite formation: an update. Geochim. Cosmochim. Acta 48, 605–615.

Berner, R.A., Raiswell, R., 1983. Burial of organic carbon and pyrite sulfur in sediments over Phanerozoic time: a new theory. Geochim. Cosmochim. Acta 47, 855–862.

Berner, R.A., Baldwin, T., Holdren Jr, G.R. 1979. Authigenic iron sulfides as paleosalinity indicators. J. Sediment. Petrol. 49, 1345–1350.

Blatt, H., Middleton, G., Murray, R., 1984. Mudrocks. Origin of Sedimentary Rocks. Prentice-Hall, Englewood Cliffs, NJ, pp. 381–409.

Canfield, D.E., 1989. Reactive iron in marine sediments. Geochim. Cosmochim. Acta 53, 619–632.

Canfield, D.E., Berner, R.A., 1987. Dissolution and pyritization of magnetite in anoxic marine sediment. Geochim. Cosmochim. Acta 51, 645–659.

Canfield, D.E., Raiswell, R., Bottrell, S., 1992. The reactivity of sedimentary iron minerals toward sulfide. Am. J. Sci. 292, 659–683.

Chen, M.P., Leu, T.C., 1984. Paleomagnetic inclination variations in Taiwan Strait after Holocene transgression. Acta Oceanogr. Taiwanica 15, 53–70.

Chester, R., Thomas, A., Lin, F.J., Basaham, A.S., Jacinto, G., 1988. The solid state speciation of copper in surface water particulates and oceanic sediments. Mar. Chem. 24, 261–292.

Davis, H.R., Byers, C.W., Dean, W.E., 1988. Pyrite formation in the lower Cretaceous Mowry shale: effect of organic matter type and reactive iron content. Am. J. Sci. 288, 873–890.

Dinarès-Turell, J., Dekkers, M.J., 1999. Diagenesis and remanence acquisition in the Lower Pliocene Trubi marls at Punta di Maiata (southern Sicily): palaeomagnetic and rock magnetic observations. In: Tarling, D.H., Turner, P. (Eds.), Palaeomagnetism and Diagenesis in Sediments. Geol. Soc. London Spec. Publ., vol. 151, 53–69.

Florindo, F., Sagnotti, L., 1995. Palaeomagnetism and rock magnetism in the upper Pliocene Valle Ricca (Rome, Italy) section. Geophys. J. Int. 123, 340–354.

Garrels, R.M., Christ, C.L., 1965. Solutions, Minerals, and Equilibria. Harper, New York. 450 pp.

Goldhaber, M.B., Kaplan, I.R., 1974. The sulfur cycle. In: Goldberg, E.D. (Ed.), The Sea, vol. 5. Wiley. New York, pp. 569–656.

Hallam, D.F., Maher, B.A., 1994. A record of reversed polarity carried by the iron sulphide greigite in British early Pleistocene sediments. Earth Planet. Sci Lett. 121, 71–80.

Hilton, J., 1990. Greigite and the magnetic properties of sediments. Limnol. Oceanogr. 35, 509–520.

Horng, C.S., Chen, J.C., Lee, T.Q., 1992a. Variations in magnetic minerals from two Plio-Pleistocene marine-deposited sections, southwestern Taiwan. J. Geol. Soc. China 35, 323–335.

Horng, C.S., Laj, C., Lee, T.Q., Chen, J.C., 1992b. Magnetic characteristics of sedimentary rocks from the Tsengwen Hsi and Erhjen Hsi sections in southwestern Taiwan. Terr. Atmos. Ocean. Sci. 3, 519–532.

Horng, C.S., Torii, M., Shea, K.S., Kao, S.J., 1998. Inconsistent magnetic polarities between greigite- and pyrrhotite/magnetite-bearing marine sediments from the Tsailiao-chi section, southwestern Taiwan. Earth Planet. Sci. Lett. 164, 467–481.

Hsu, S.C., Lin, F.J., Jeng, W.L., Chung, Y.C., Shaw, L.M., 2003. Hydrothermal signatures in the southern Okinawa Trough detected by the sequential extraction of settling particles. Mar. Chem. 84 (1), 49–66.

Huang, K.M., Lin, S., 1995. The carbon–sulfide–iron relationship and sulfate reduction rate in the East China Sea continental shelf sediments. Geochem. J. 29, 301–315.

Jelinowska, A., Tucholka, P., Gasse, F., Fontes, J.C., 1995. Mineral magnetic record of environment in Late Pleistocene and Holocene sediments, Lake Manas, Xinjiang, China. Geophys. Res. Lett. 22, 953–956.

Jiang, W.T., Horng, C.S., Roberts, A.P., Peacor, D.R., 2001. Contradictory magnetic polarities in sediments and variable timing of neoformation of authigenic greigite. Earth Planet. Sci. Lett. 193, 1–12.

Kalcheva, V., Nozharov, P., Kovacheva, M., Shopov, V., 1990. Paleomagnetic research on Black Sea Quaternary sediments. Phys. Earth Planet. Inter. 63, 113–120.

Kokot, S., King, G., Leller, H.R., Massart, D.L., 1992. Application of chemometrics for the selection of microwave digestion procedures. Anal. Chim. Acta 268, 81–94.

Krs, M., Krsova, M., Pruner, P., Zeman, A., Novak, F., Jansa, J., 1990. A petromagnetic study of Miocene rocks bearing microorganic material and the magnetic mineral greigite (Sokolov and Cheb basins Czechoslovakia). Phys. Earth Planet. Inter. 63, 98–112.

Lee, T., You, C.F., Liu, T.K., 1993. Model-dependent ^{10}Be sedimentation rates for the Taiwan Strait and their tectonic significance. Geology 21, 423–426.

Lin, S., Morse, J.W., 1991. Sulfate reduction and iron sulfide mineral formation in Gulf of Mexico anoxic sediments. Am. J. Sci. 291, 55–89.

Linssen, J.H., 1988. Preliminary results of a study of four successive sedimentary geomagnetic reversal records from the Mediterranean (Upper Thvera, Lower and Upper Siduf-jall, and Lower Nunivak). Phys. Earth Planet. Inter. 52, 207–231.

Mary, C., Iaccarino, S., Courtillot, V., Besse, J., Aïssaoui, D.M., 1993. Magnetostratigraphy of Pliocene sediments from the Stirone River (Po Valley). Geophys. J. Int. 112, 359–380.

Morse, J.W., Millero, F.J., Cornwell, J.C., Rickard, D., 1987. The chemistry of the hydrogen sulfide and iron sulfide system in natural waters. Earth Sci. Rev. 24, 1–42.

Raiswell, R., Berner, R.A., 1986. Pyrite and organic-matter in Phanerozoic normal marine shales. Geochim. Cosmochim. Acta 50, 1967–1976.

Raiswell, R., Canfield, D.E., 1996. Rates of reaction between silicate iron and dissolved sulfide in Peru Margin sediments. Geochim. Cosmochim. Acta 60, 2777–2787.

Raiswell, R., Canfield, D.E., 1998. Sources of iron for pyrite formation in marine sediments. Am. J. Sci. 298, 219–245.

Raiswell, R., Canfield, D.E., Berner, R.A., 1994. A comparison of iron extraction methods for the determination of degree of pyritization and the recognition of iron-limited pyrite formation. Chem. Geol. 111, 101–110.

Reynolds, R.L., Tuttle, M.L., Rice, C.A., Fishman, N.S., Karachewski, J.A., Sherman, D.M., 1994. Magnetization and geochemistry of greigite-bearing Cretaceous strata, North Slope Basin, Alaska. Am. J. Sci. 294, 485–528.

Roberts, A.P., Turner, G.M., 1993. Diagenetic formation of ferrimagnetic iron sulphide minerals in rapidly deposited marine sediments, New Zealand. Earth Planet. Sci. Lett. 115, 257–273.

Roberts, A.P., Reynolds, R.L., Verosub, K.L., Adam, D.P., 1996. Environmental magnetic implications of greigite (Fe_3S_4) formation in a 3 m.y. lake sediment record from Butte Valley, northern California. Geophys. Res. Lett. 23, 2859–2862.

Sagnotti, L., Winkler, A., 1999. Rock magnetism and palaeomagnetism of greigite-bearing mudstones in the Italian peninsula. Earth Planet. Sci. Lett. 165, 67–80.

Schoonen, M.A.A., Barnes, H.L., 1991a. Reactions forming pyrite and marcasite from solution: I. Nucleation of FeS_2 below 100°C. Geochim. Cosmochim. Acta 55, 1495–1504.

Schoonen, M.A.A., Barnes, H.L., 1991b. Reactions forming pyrite

and marcasite from solution: II. Via FeS precursors below 100 °C. Geochim. Cosmochim. Acta 55, 1505–1514.

Snowball, I.F., 1991. Magnetic hysteresis properties of greigite (Fe_3S_4) and a new occurrence in Holocene sediments from Swedish Lappland. Phys. Earth Planet. Inter. 68, 32–40.

Snowball, I.F., Thompson, R., 1988. The occurrence of greigite in sediments from Loch Lomond. J. Quat. Sci. 3, 121–125.

Snowball, I.F., Thompson, R., 1990. A stable chemical remanence in Holocene sediments. J. Geophys. Res. 95, 4471–4479.

Sweeney, R.E., Kaplan, I.R., 1973. Pyrite framboid formation: laboratory synthesis and marine sediments. Econ. Geol. 5, 618–634.

Torii, M., Fukuma, K., Horng, C.S., Lee, T.Q., 1996. Magnetic discrimination of pyrrhotite- and greigite-bearing sediment samples. Geophys. Res. Lett. 23, 1813–1816.

Tric, E., Laj, C., Jehanno, C., Valet, J.-P., Kissel, C., Mazaud, A., Iaccarino, S., 1991. High-resolution record of the Upper Olduvai transition from Po Valley (Italy) sediments: support for dipolar transition geometry? Phys. Earth Planet. Inter. 65, 319–336.

Tsai, S.W., Chung, Y., 1989. Pb-210 in the sediments of Taiwan Strait. Acta Oceanogr. Taiwanica 22, 1–13.

Tsai, C.H., Rau, S.R., 1992. Evaluation of Galai CIS-1 for measuring size distribution of suspended primary particles in the ocean. Terr. Atmos. Ocean. Sci. 3, 147–164.

Tseng, J.M., 1991. Study on speciation of trace metals in sediments, MS Thesis, National Taiwan University, Taipei, Taiwan (in Chinese).

Tyson, R.V., 2001. Sedimentation rate, dilution, preservation and total organic carbon: some results of a modeling study. Org. Geochem. 32, 333–339.

Weaver, R., Roberts, A.P., Barker, A.J., 2002. A late diagenetic (syn-folding) magnetization carried by pyrrhotite: implications for paleomagnetic studies from magnetic iron sulphide-bearing sediments. Earth Planet. Sci. Lett. 200, 371–386.

Wilkin, R.T., Barnes, H.L., 1997. Pyrite formation in an anoxic estuarine basin. Am. J. Sci. 297, 620–650.